AGU PUBLICATIONS

JGR

Journal of Geophysical Research: Atmospheres

RESEARCH ARTICLE
10.1002/2017JD027606

Key Points:
- The Integrated Multi-Satellite Retrievals for GPM is evaluated and compared with the TRMM real-time product over the United States
- IMERG improves upon TMPA-RT in terms of miss-rain, false-rain bias reduction, and hit rate as a result of a reduced use of IR
- It confirms the advances of the new generation algorithm relative to its predecessor and highlight areas requiring additional investigation

Correspondence to:
P.-E. Kirstetter,
pierre.kirstetter@noaa.gov

Citation:
Gebregiorgis, A. S., Kirstetter, P.-E., Hong, Y. E., Gourley, J. J., Huffman, G. J., Petersen, W. A., Xue, X., … Schwaller, M. R. (2018). To what extent is the day 1 GPM IMERG satellite precipitation estimate improved as compared to TRMM TMPA-RT?. *Journal of Geophysical Research: Atmospheres*, *123*, 1694–1707. https://doi.org/10.1002/2017JD027606

Received 15 AUG 2017
Accepted 7 JAN 2018
Accepted article online 22 JAN 2018
Published online 6 FEB 2018

To What Extent is the Day 1 GPM IMERG Satellite Precipitation Estimate Improved as Compared to TRMM TMPA-RT?

Abebe S. Gebregiorgis[1,2,3], Pierre-Emmanuel Kirstetter[2,3,4], Yang E. Hong[2,3], Jonathan J. Gourley[4], George J. Huffman[5], Walter A. Petersen[6], Xianwu Xue[2,3], and Mathew R. Schwaller[6]

[1]Harris County Flood Control District, Houston, TX, USA, [2]School of Civil Engineering and Environmental Sciences, University of Oklahoma, Norman, OK, USA, [3]Advanced Radar Research Center, University of Oklahoma, Norman, OK, USA, [4]NOAA/National Severe Storms Laboratory, Norman, OK, USA, [5]NASA Goddard Space Flight Center, Greenbelt, MD, USA, [6]NASA Marshall Space Flight Center, Huntsville, AL, USA

Abstract Integrated Multi-Satellite Retrievals for Global Precipitation Measurement (IMERG) is the last generation precipitation data source for a wide array of research, operational, and societal applications. The Global Precipitation Measurement mission provides these global and high-resolution precipitation estimates through advanced satellite-based radar and radiometers. The degree of improvement of the new IMERG products needs to be investigated to further advance the algorithm's development and application. This study focuses on systematically and extensively evaluating the uncalibrated Version 3 Late Run IMERG product, which has both backward and forward morphing, and highlights the level of improvement in comparison to its predecessor Version 7 Tropical Rainfall Measurement Mission (TRMM)-based Multi-satellite Precipitation Analysis real-time product. Retrievals from different passive microwave (PMW) and infrared (IR) sensors contributing to IMERG are evaluated over the conterminous United States using ground-based sensor precipitation estimates derived from the Multi-Radar Multi-Sensor system as reference. An error decomposition scheme is implemented to separate the total error into three independent components, hit, miss-rain, and false-rain biases, to trace the degree of improvement of the new algorithm. IMERG exhibits definite improvement related to miss-rain and false-rain bias reduction and hit rate. The improvement relative to the TRMM -IR component is more substantial than relative to the PMW retrieval as a result of the new Kalman smoother and the PMW morphing reducing the use of IR relative to the TRMM-based Multi-satellite Precipitation Analysis. Findings of this study confirm the advances of the new generation of multisatellite precipitation relative to its predecessor and highlight areas requiring additional investigation.

1. Introduction

Evaluating satellite precipitation estimates has remained an important task to improve the quality of these data and ultimately advance their use for a variety of applications such as hydrologic and meteorological applications, flood forecasting, transboundary water resources modeling, global/regional drought, and agricultural planning (Turk et al., 2010). The validation of satellite precipitation estimates is conventionally performed by comparing with ground observations (including gauges and radar) since this provides the most realistic picture of the rain rate on the ground where the surface data are sufficiently dense and reliable (Kirstetter et al., 2014; Wolff et al., 2005; Zhang et al., 2015). The validation of satellite precipitation estimates over diverse topographic and climatic regions helps to evaluate their accuracy and identify specific weaknesses requiring attention and strengths of the product under different circumstances.

Over the past two decades several studies have been conducted on the validation of satellite precipitation estimates with available ground truth data to ascertain their accuracy over various continents and space and time scales (Curtis et al., 2007; Dinku et al., 2007; Ebert et al., 2007; Gottschalck et al., 2005; Gebregiorgis & Hossain, 2014; Gebregiorgis et al., 2017; Hong et al., 2007; Huffman et al., 2007; Kirstetter et al., 2012, 2014, 2015, 2017; Ruane & Roads, 2007; Sapiano & Arkin, 2008; Tang et al., 2014; Tian et al., 2007; among many others). For instance, Gottschalck et al. (2005) showed that the Tropical Rainfall Measurement Mission (TRMM)-based Multi-satellite Precipitation Analysis (TMPA) real-time product (3B42RT) tends to overestimate over the central United States, which is attributed to cold cirrus clouds

misclassified as precipitating systems. Dinku et al. (2008) noted that topography plays a significant role in satellite precipitation estimation due to the algorithm's weakness to detect orographically induced precipitation. Gebregiorgis and Hossain (2014) pointed out that topography and climate are some of the key governing factors to characterize the uncertainty of satellite precipitation products.

In this study, the shift in accuracy in satellite precipitation estimates from the TRMM to the Global Precipitation Measurement (GPM) era is investigated by comparing the Integrated Multi-Satellite Retrievals for Global Precipitation Measurement (IMERG) Late Run to its predecessor TMPA. The GPM mission started to provide global precipitation estimates at fine spatiotemporal resolution on 12 March 2014. From the perspective of both data users and producers it is important to assess its performance over several seasons to advance its applications and improve the quality of data.

The question motivating this study is "To what extent have the IMERG multisatellite precipitation estimate improved as compared to its predecessor, TMPA-real time (RT)?" To this end the precipitation estimates originating from passive microwave (PMW) and infrared (IR) sensors contributing to the combined estimates are segregated and assessed independently. The total error is decomposed into detection and estimation bias components in order to assess the algorithm performance at different retrieval stages. The strengths and weaknesses of both algorithms are assessed in a variety of settings to comprehensively evaluate the performance of the IMERG algorithm and assist with highlighting aspects that are in greater need of improvement.

The availability of reference data is a decisive factor in choosing the study region. The conterminous United States (CONUS) is among the best regions in the world to perform precipitation validation because dense and well-maintained gauge and weather radar networks are available (Kirstetter et al., 2012). The Multi-Radar Multi-Sensor system (MRMS) developed at the National Oceanic and Atmospheric Administration National Severe Storms Laboratory ingests data from all ground-based radars comprising the Weather Surveillance Radar-1988 Doppler network, intelligently combines the information, and provides high-resolution precipitation rate mosaics over the CONUS (Zhang et al., 2015).

The CONUS provides diverse topographic and climatic features. The physiographic conditions range from lowland and flat floodplains to high mountains and variable climate and weather conditions. The precipitation climatologies differ significantly across the states with, for example, significant contributions from tropical cyclones and convective systems across the eastern and southeast regions and orographic precipitation in the complex terrain of the Intermountain West. These diverse physiographic and meteorological features make the CONUS a valuable test bed to conduct the evaluation of satellite precipitation products.

The paper is organized as follows. Section 2 describes the TMPA-RT and IMERG algorithms as well as the radar precipitation data sets used. Section 3 discusses the key findings associated with the TMPA-RT and IMERG precipitation estimates, the error structure, and the degree of improvement achieved in the IMERG product. Conclusions and recommendations for future studies are provided in the last section.

2. Algorithms, Data Descriptions, and Methodology

2.1. TMPA-RT and IMERG Algorithms

The TMPA-RT rainfall estimate is a combination of PMW and IR sensors estimates. The major difference between the two types of sensors lies in the principle and precipitation measurement technique. For IR sensors, the precipitation at the ground is related to cloud top brightness temperature observed from space (Levizzani et al., 2002). PMW retrievals use the principle that precipitation at the surface is related to microwave (MW) emission from raindrops at low-frequency channels and MW scattering from ice at high-frequency channels (Kummerow et al., 1998). The PMW sensors benefit from a more direct physical connection to the hydrometeor profiles but have poor temporal sampling because they fly on low Earth orbit satellites, whereas IR sensors on board geostationary satellite platforms have excellent time-space resolution and coverage but indirect relationship to surface precipitation. Therefore, the TMPA-RT merging process is designed to exploit the complementary advantages obtained from the two sensors: accuracy and best spatial resolution and sampling frequency.

Figure 1a shows the flowchart of TMPA-RT algorithm. The 2B31 level II product is a combined precipitation profile derived from the TRMM precipitation radar reflectivity (1C21) and the TRMM Microwave Imager calibrated brightness temperature (1B11) and is used to calibrate the instantaneous PMW precipitation estimates (Huffman & Bolvin, 2015). Subsequent high-quality PMW-only precipitation estimates are created to locally

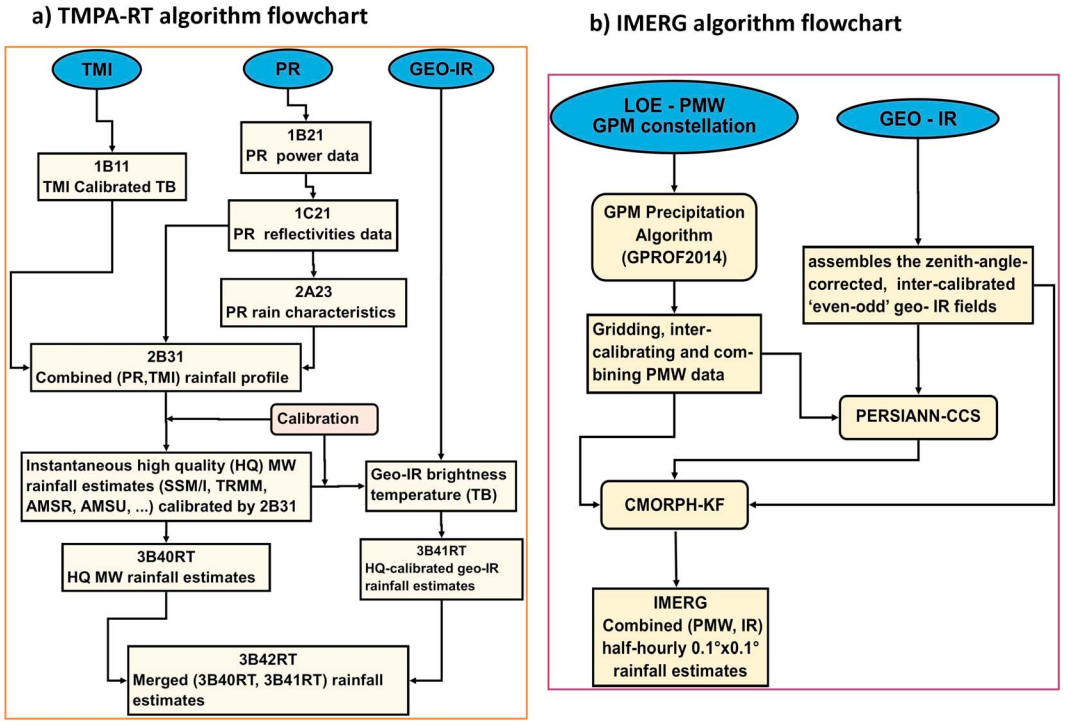

Figure 1. Flowcharts of (a) Tropical Rainfall Measurement Mission-based Multi-satellite Precipitation Analysis real-time product (TMPA-RT) and (b) Integrated Multi-Satellite Retrievals for Global Precipitation Measurement (IMERG) algorithms.

calibrate IR precipitation estimates. The IR precipitation estimation is a simple "colder clouds is more likely to rain" approach, with the coldest 0.25° × 0.25° average T_b assigned directly the greatest observed PMW precipitation rate. The intersatellite calibration of the high-quality product has more accurate long-term climate data records from different radiometers than just using single-satellite estimates. The calibrated IR precipitation estimates are used to fill the PMW coverage gaps (Huffman et al., 2007, 2010) to produce the merged satellite precipitation product (3B42RT) at 0.25° spatial and 3 h temporal resolutions.

Building upon the success of TRMM, the GPM Core Observatory satellite was launched on 28 February 2014. The core satellite carries the spaceborne dual-frequency phased array precipitation radar operating at Ku and Ka bands (13.6 and 35.5 GHz, respectively) and a conical-scanning multichannel (10–183 GHz) MW imager. This set of instruments is used to generate combined active-passive precipitation profiles and calibrate the retrievals from other satellite platforms. As a successor of TMPA, IMERG is a unified satellite algorithm developed to provide a multisatellite precipitation product over nearly the entire globe. Like the TRMM algorithm, the sources of precipitation information originate from the same low-orbiting platforms and the geostationary satellites.

The precipitation estimates from the various PMW and IR sensors are gridded, intercalibrated, and assembled into half-hourly 0.1° × 0.1° fields. Figure 1b illustrates the major processing modules and data flows in the IMERG algorithm (Huffman et al., 2014, 2015). Compared to TMPA, the PMW precipitation estimates are all computed using a new-generation Goddard Profiling Algorithm (GPROF) that uses the full brightness temperature vector to obtain the most likely precipitation field (Kummerow et al., 2015). The fundamental concept of the algorithm is a Bayesian approach. The output of GPROF is gridded, intercalibrated, and combined into half-hourly PMW multisensors product. These combined precipitation estimates are then provided to both the Precipitation Estimation from Remotely Sensed Information using Artificial Neural Networks-Cloud Classification System (PERSIANN-CCS; Hong et al., 2004) computation routines and the Climate Prediction Center Morphing-Kalman Filter (CMORPH-KF, Joyce & Xie, 2011) Lagrangian time interpolation scheme.

The PERSIANN-CCS (Hong et al., 2004) was designed to improve the relationship between the IR brightness temperature field (T_b) and surface precipitation. It uses cloud image segmentation, cloud patch features

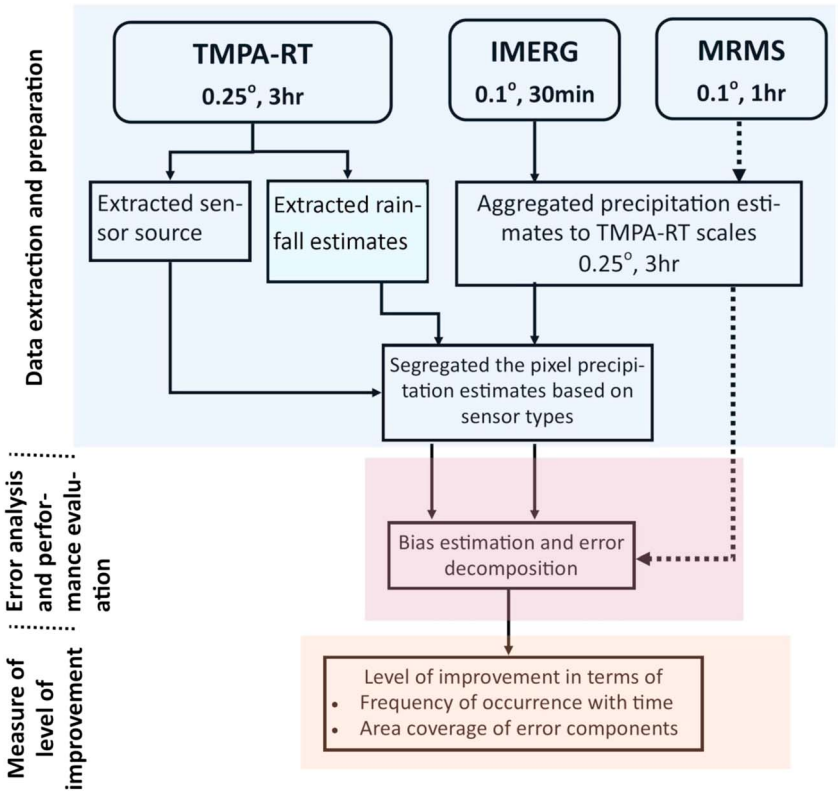

Figure 2. Processing stages for error analysis and level improvement between Tropical Rainfall Measurement Mission-based Multi-satellite Precipitation Analysis real-time product (TMPA-RT) and Integrated Multi-Satellite Retrievals for Global Precipitation Measurement (IMERG) precipitation products.

extraction, cloud patches classification, and cloud patch precipitation estimation schemes. The IR image is segmented using gradually increasing thresholds temperature (220 K, 235 K, and 253 K) to extract the convective cloud patch features at different altitudes considering the temperature, geometry, and texture of the clouds. To classify the extracted cloud patch features into different patch groups, an unsupervised clustering algorithm is implemented. Finally, a cloud precipitation function is optimized to each cloud patch group based on a training set of the collocated PMW precipitation using power law regression and histogram matching to derive the parameters with respect to each group.

The CMORPH-KF algorithm used in IMERG is similar to the current scheme in CMORPH and related to that in GSMap. It involves estimating cloud motion fields from geo-IR data, moving PMW multisensors swath data using the computed displacements, and applying a Kalman smoothing to combine satellite data displaced from nearby times. This Lagrangian time interpolation scheme (Joyce & Xie, 2011) propagates the intercalibrated PMW precipitation features forward and backward in time using the cloud motion vectors obtained from the geo-IR images. It mitigates PMW coverage gaps in the TMPA algorithm. Then the propagated features are morphed by linearly interpolating in time to create half-hourly 0.1° × 0.1° fields from the PMW and IR estimates. The IR estimates are weighted into the Kalman smoother when their estimated correlation is close to that of the morphed PMW estimates.

2.2. Data Description

Building on the TMPA processing concept, the IMERG product has multiple runs aiming to serve different users' needs for timeliness. The "early" multisatellite product is the first, quick precipitation estimate, with ~4 h latency after observation time (the product is available at https%3A%2F%2Fpmm.nasa.gov%2Fdata-access%2Fdownloads%2Fgpm). This product is intended for flood applications and precipitation nowcasting purposes. The "late" multisatellite product waits to include PMW data for backward propagation, resulting in ~14 h delay after observation. This product targets operational users such as crop, flood, and drought analysts. Once the monthly gauge precipitation analysis is received, the "final" best

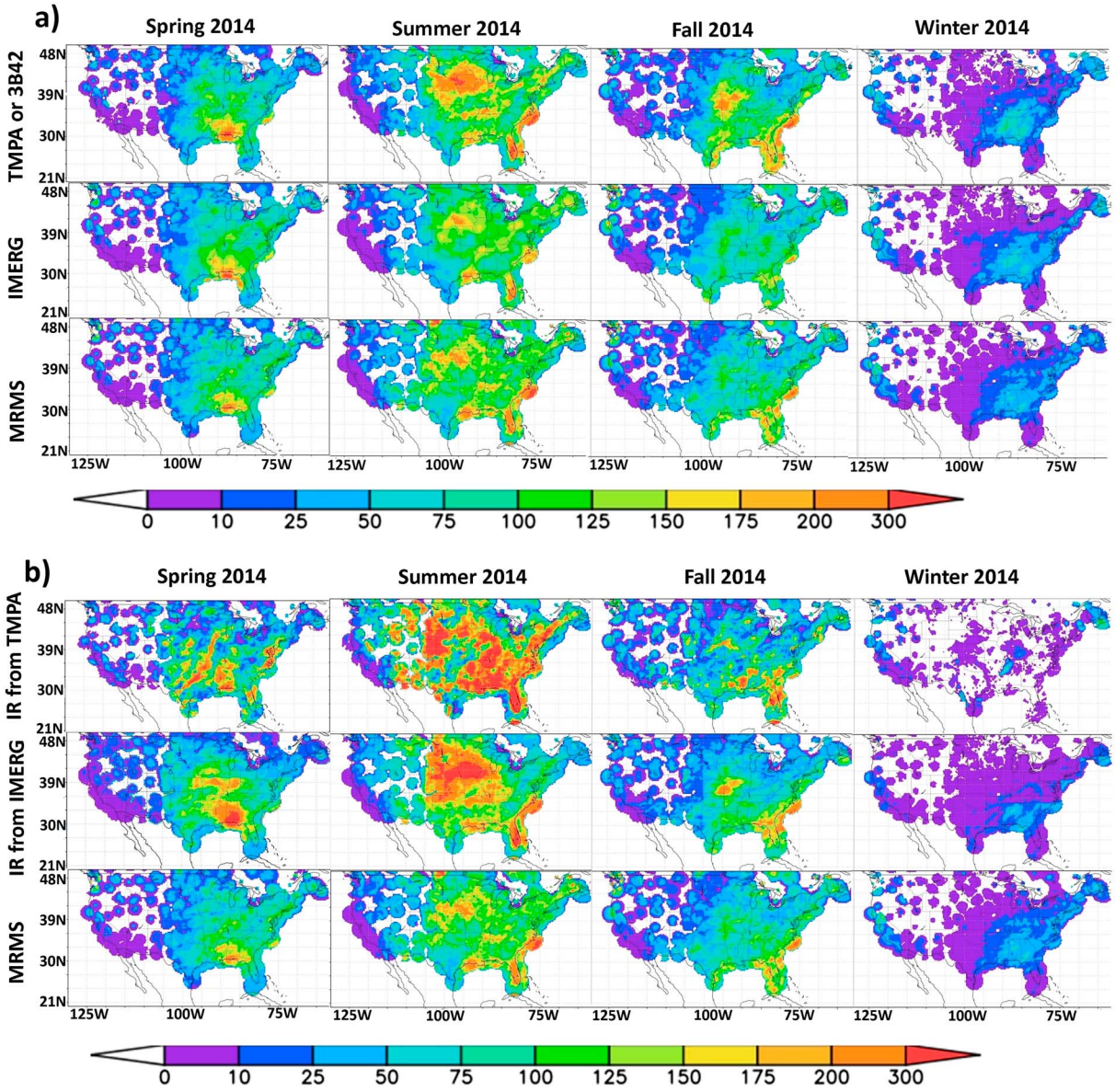

Figure 3. Spatial distribution of seasonal cumulative precipitation (mm) for Tropical Rainfall Measurement Mission-based Multi-satellite Precipitation Analysis real-time product (TMPA-RT), Integrated Multi-Satellite Retrievals for Global Precipitation Measurement (IMERG), and Multi-Radar Multi-Sensor system (MRMS) precipitation estimates for (a) merged infrared (IR) and passive microwave (MW) sensors and (b) IR-only sensors.

satellite gauge product is assembled with about 3 months latency after observation. All of the runs provide multiple fields that provide information on the input data, selected intermediate fields, and estimation quality. Such information helps to ensure data processing traceability and support for algorithm studies. In this study, the late run multisatellite precipitation product is evaluated during the study period of 2014. To avoid the climatological monthly gauge correction, the uncalibrated precipitation data field is chosen.

A high-resolution ground-based radar precipitation reference data set derived from MRMS (Kirstetter et al., 2012) is used to evaluate the performance of both IMERG and TMPA-RT products. MRMS uses advanced quality control and data integration techniques to create consistent and accurate precipitation estimates (the product is available at http://mrms.ncep.noaa.gov/data). The MRMS ingests data from the NEXRAD radar network to create high-resolution 3-D reflectivity mosaic grids and quantitative precipitation estimates products over the CONUS at 0.01° spatial and 2 min temporal scales (Zhang et al., 2011, 2015). MRMS is currently the finest-

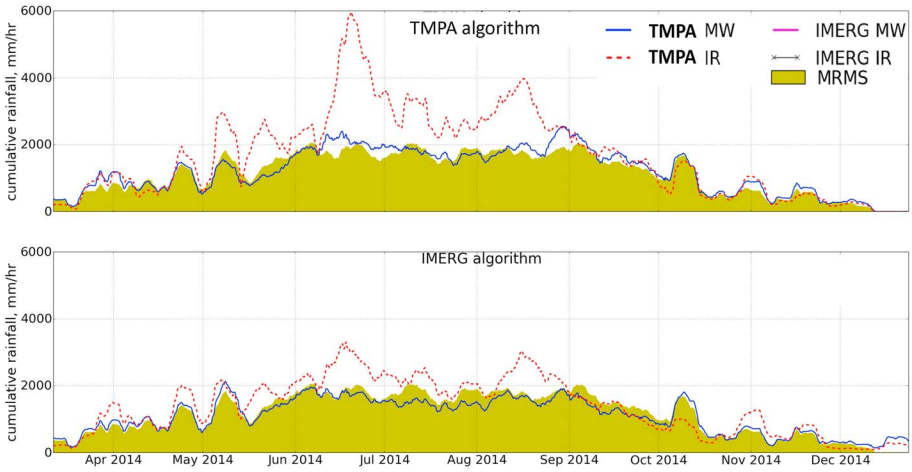

Figure 4. Comparison of cumulative precipitation estimates (mm) originating from passive microwave (MW) and infrared (IR) of Tropical Rainfall Measurement Mission-based Multi-satellite Precipitation Analysis real-time product (TMPA-RT) and corresponding Integrated Multi-Satellite Retrievals for Global Precipitation Measurement (IMERG) grid boxes.

scale operational ground precipitation product and is being utilized by different public institutions, universities, and in the private sector for hydrometeorological applications. In evaluating satellite precipitation products with an exogenous reference, the quality of the reference data set is a key factor to get the most realistic picture of the true state and draw meaningful conclusions. The reference precipitation is generated through significant MRMS data postprocessing, involving gauge-based bias adjustments, resampling, and quality controls as described in Kirstetter et al. (2012, 2014, 2015). It only retains the most trustworthy, best quality precipitation estimates at the hourly time scale. This conservative approach is designed to homogenize the reference quality and has a significant impact on the availability of data specifically in the Intermountain West, where the quality of radar measurements tends to be lower than in other regions of the country.

2.3. Methodology

The methodology of the study is briefly described in Figure 2. Two data fields are extracted from TMPA-RT: the sensor source and the precipitation estimates. The TMPA-RT sensor source classifies the pixel precipitation estimates into different sensor groups for every 0.25°/3 h grid box value over the CONUS. Note that the TMPA-RT precipitation estimates are pure IR or PMW estimates. While the IMERG products originate from the same constellation of satellite sensors, the IMERG precipitation estimates are weighted combinations of IR and PMW estimates, especially in TMPA-RT IR pixels. In this analysis, the TMPA-RT sensor source is the basis for classifying pixel precipitation estimates from TMPA-RT, MRMS, and IMERG into different sensor groups. The IMERG and MRMS products are consistently remapped to match the grid scale of TMPA-RT at 0.25° and 3-hourly. Spatial aggregation from 0.1° to 0.25° has been made using the cubic convolution resampling method, which is based on the weighted average of 16 nearest neighboring pixels to generate new values. By conditioning the analysis according to the TMPA-RT sensor source, the improvement of IMERG relative to TMPA is evaluated (rather than compared independently).

To gain more insight on the source and type of errors that characterize PMW and IR estimates in both products, it is desirable to decompose the overall bias into three independent components (Tian et al., 2009; see Appendix A). These error components consist of the bias associated with successful detections (hit/estimation bias), precipitation misses (missed-rain bias), and false detection (false-rain bias). To visualize the improvement between the two satellite precipitation products, two performance measures are applied. First, the frequency of occurrence of each error component in TMPA-RT and IMERG products is computed as percentage over the study period for each individual 0.25° grid box. Second, the percentage of extent of area coverage of each error components is computed for both precipitation products. The level of improvement is evaluated based on percent change of occurrence and extent of area coverage of hit, miss, and false rain over the CONUS.

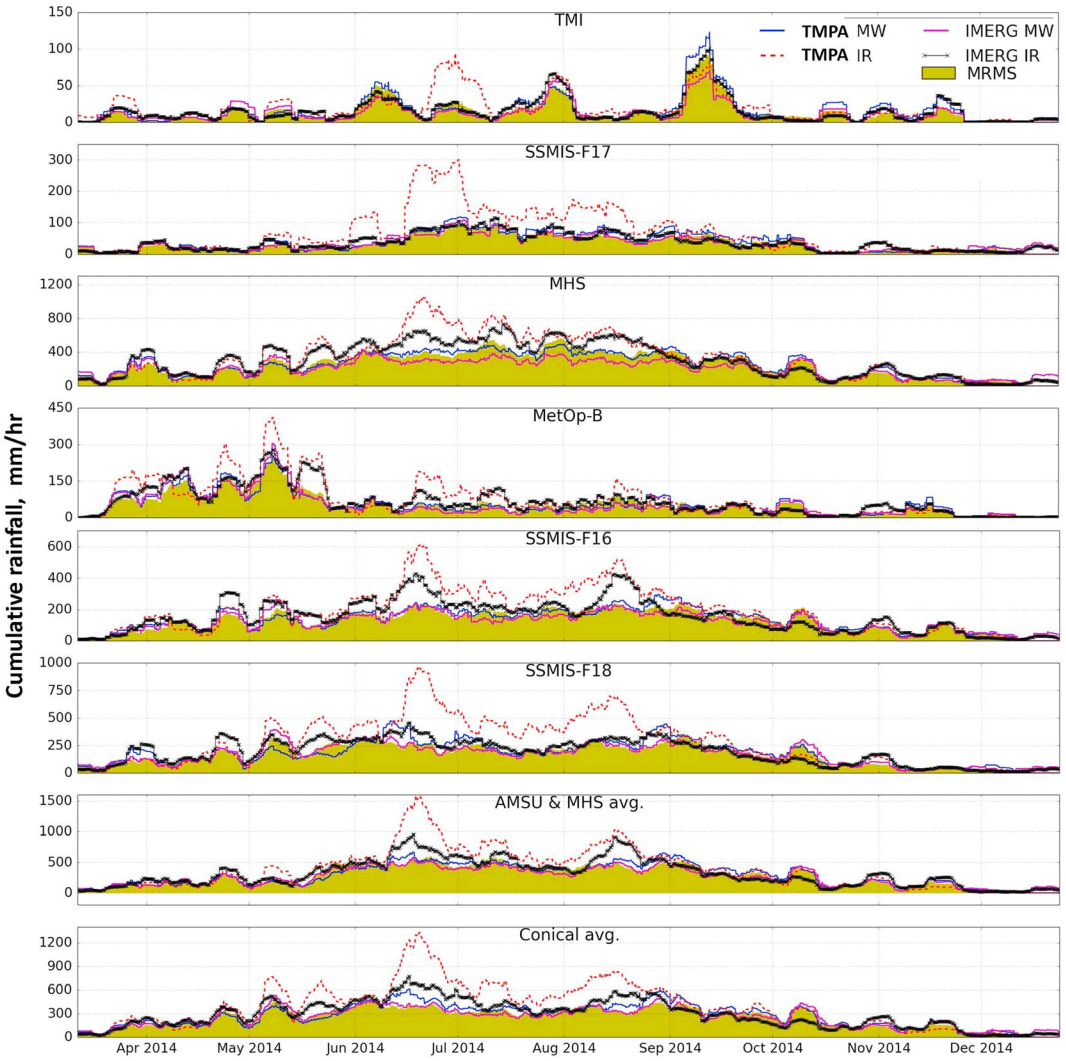

Figure 5. Time series of cumulative precipitation (mm) estimates originated from the available passive microwave (MW) sensors of Tropical Rainfall Measurement Mission-based Multi-satellite Precipitation Analysis real-time product (TMPA-RT) and corresponding TMPA-RT, Integrated Multi-Satellite Retrievals for Global Precipitation Measurement (IMERG), and Multi-Radar Multi-Sensor system (MRMS) precipitation grid box estimates.

3. Results and Discussion

Precipitation types vary significantly across the United States. The West, Northwest, and Northeast have more stratiform precipitation, while the Midwest and central United States are dominated by convective precipitation. The South and Southeast receive comparably higher contribution from tropical and warm rain (Chen et al., 2015). Figure 3 illustrates the spatial distribution of seasonal cumulative precipitation for Version 7 TMPA-RT, Version 03 IMERG Late Run, and MRMS precipitation estimates during the study period (2014). The combined PMW and IR products are shown in Figure 3a, and the estimates coincident with TMPA IR-only are shown in Figure 3b for comparison. TMPA-RT overestimates the precipitation amounts, specifically in the north central United States during spring, summer, and fall. In general, IMERG is more consistent with the reference for all seasons, except for a slight underestimation over Florida and the southeast coastal region of the CONUS during fall. The TMPA-RT overestimation is likely due to the IR-based retrievals as shown in Figure 3b. The inclusion of IR data into both TMPA and IMERG algorithms results in considerable overestimation (although in IMERG it is slightly less and localized) in all seasons except winter (Figure 3b). The improvement from TMPA to IMERG is significant in winter. IR precipitation estimation is indirectly inferred from cloud top temperature and has limited accuracy for detection/quantification of cold precipitation.

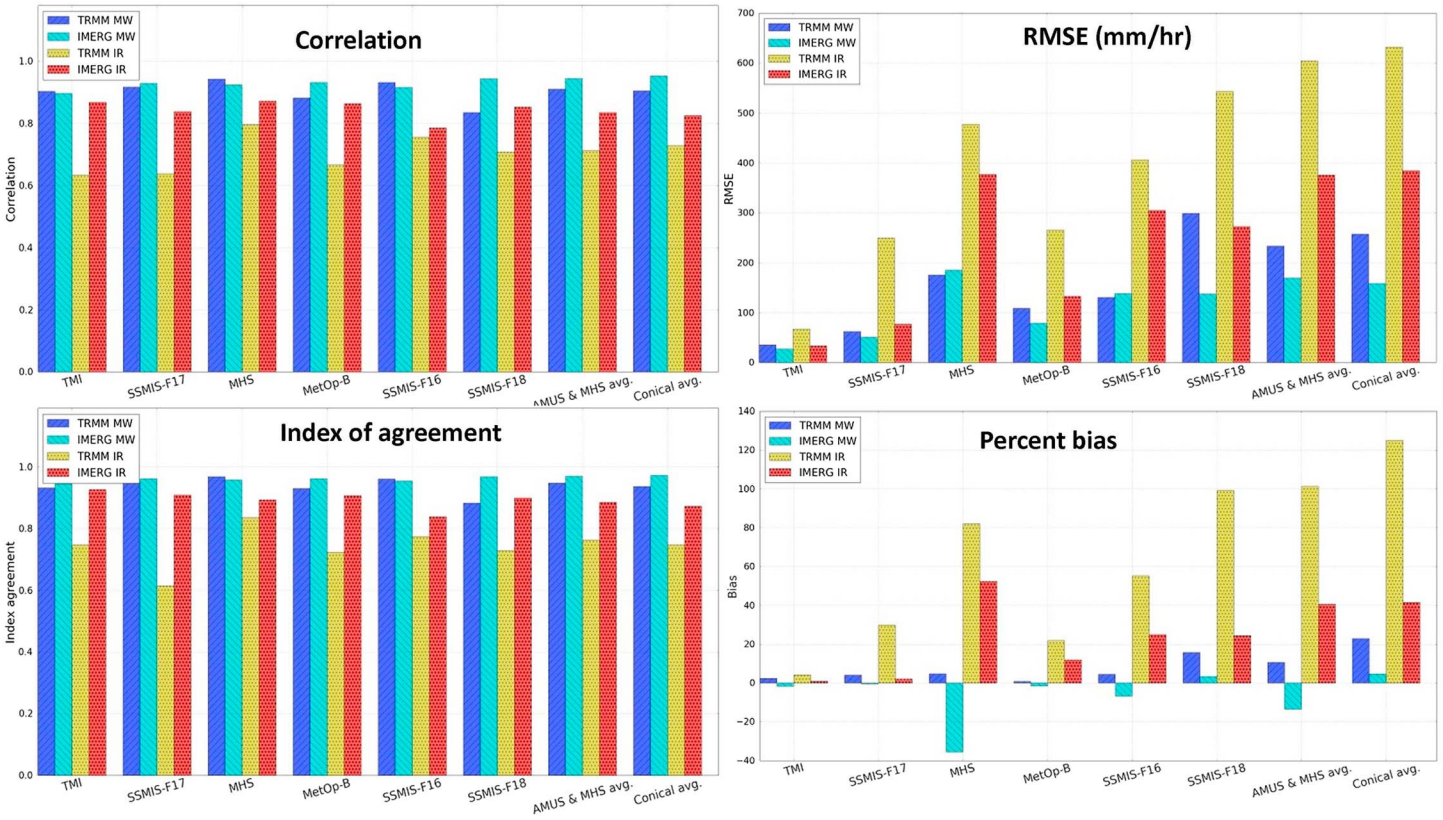

Figure 6. Correlation, root mean square error (RMSE), index of agreement, and percent bias of passive microwave (MW) and infrared (IR) precipitation estimates contained in the Tropical Rainfall Measurement Mission-based Multi-satellite Precipitation Analysis real-time product (TMPA-RT) and Integrated Multi-Satellite Retrievals for Global Precipitation Measurement (IMERG) data sets.

IR-based precipitation estimates present substantial uncertainties that propagate into the final MW-IR merged product (Kirstetter et al., 2017). These precipitation estimates are generated through matching the distribution of the IR T_b against the available PMW precipitation retrievals. For regions where no PMW retrieval is available, the matching tables are similar with the neighboring regions. A relatively constant calibration is performed for all precipitation events in the calibration data sample, despite the true variability that exists from event to event. Therefore, calibration with PMW reasonably improves the accuracy yet does not resolve all the uncertainties in IR retrieval techniques. The updating and the filling of the TMPA PMW coverage gaps are probably to be credited in this improved performance by IMERG. The slight overestimation with the IMERG algorithm shows that this achievement comes from an algorithm improvement as the result of the PMW morphing reducing the use of IR relative to the TMPA.

A time series of spatially aggregated precipitation over the CONUS for the PMW and IR components of TMPA and corresponding IMERG estimates are shown, along with MRMS, in Figure 4. Higher accumulations related to higher convective activity occur during the warm season. The result clearly reveals that there is a significant improvement in IMERG corresponding to TMPA grid boxes with IR estimates. This is because morphing in IMERG mitigates the PMW coverage gaps. Second, in regions where both TMPA and IMERG rely on IR, the PERSIANN-CCS and the PMW-based IR calibration in IMERG result in improved accuracy.

Figure 5 shows the time series of spatially accumulated precipitation estimates segregated according to the TMPA-RT individual PMW and IR sensors types. For the comparison between products, TMPA-RT and IMERG estimates are spatially accumulated for the corresponding PMW grid boxes. The PMW precipitation estimates from TMPA-RT and IMERG product agree reasonably well with the reference data over the entire period (2014), and the major improvement comes from the estimate in IMERG in regions of IR-based TMPA, with slight overestimation particularly during the rainy season. The bias, correlation, index of agreement, and root mean square error (RMSE) are provided according to sensor type in Figure 6 to highlight the change in the

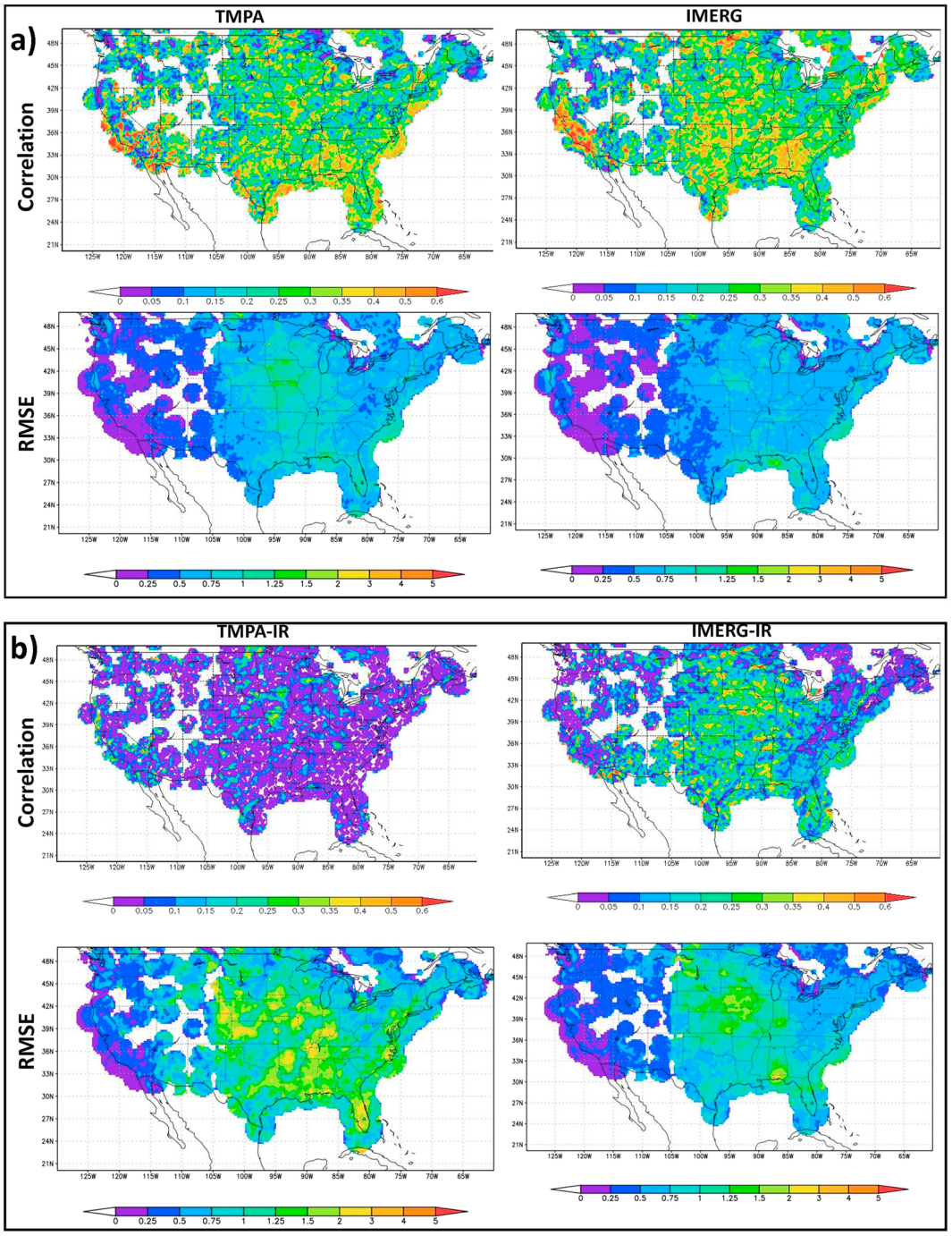

Figure 7. Correlation and RMSE for Tropical Rainfall Measurement Mission-based Multi-satellite Precipitation Analysis real-time product (TMPA-RT) (left column) and Integrated Multi-Satellite Retrievals for Global Precipitation Measurement (IMERG) (right column) (a) passive microwave (PMW) and (b) infrared (IR) precipitation estimates for 2014.

agreement with the reference from TMPA to IMERG. Correlation coefficient and index of agreement illustrate the quantitative measure of the correlation and dependence. The index of agreement can detect proportional difference in the estimated and observed means and variances. Its value varies from 0 to 1 in which the value of 1 indicates a perfect match and 0 designates no agreement (Willmott, 1981; see Appendix A).

Regarding PMW precipitation estimates, the correlation shows high values (>0.8) and is comparable between TMPA-RT and IMERG. The index of agreement tends to slightly decrease from TMPA to IMERG. The bias is

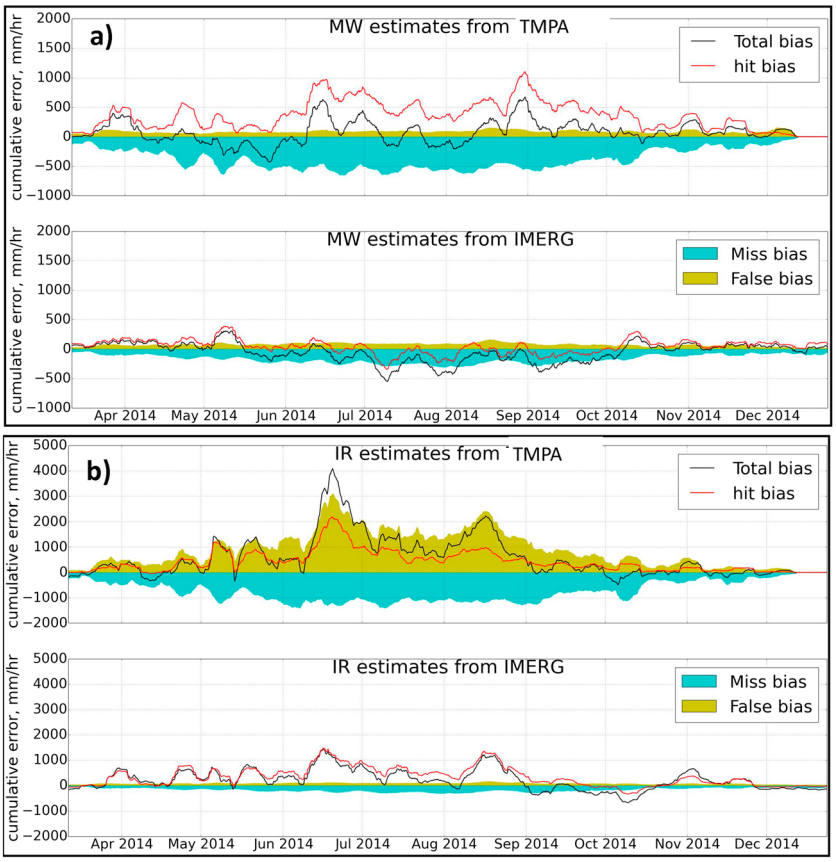

Figure 8. Error component for (a) passive microwave (MW) and (b) infrared (IR) precipitation estimates of Tropical Rainfall Measurement Mission-based Multi-satellite Precipitation Analysis real-time product (TMPA-RT) (top) and Integrated Multi-Satellite Retrievals for Global Precipitation Measurement (IMERG) (bottom) data sets.

positive for both satellite products. It increases from TMPA (range (2–18)%) to IMERG (range (8–30)%). The retrieval database of the day 1 at-launch GPROF algorithm is empirical and did not have a chance to benefit from the combined active-passive observations from the GPM Core Observatory, as has been the case in the following versions (Passive Microwave Algorithm Team Facility, PMATF, 2014). The higher bias contributes to the higher RMSE generally observed in IMERG than in TMPA-RT. Regarding IR estimates corresponding to the PMW sensors, a systematic improvement from TMPA to IMERG for all sensors and scores is noticed. As seen in Figure 6, IR from IMERG demonstrates higher performance, with both correlation and index of agreement greater than 0.8, while they range at [0.6–0.8] with TMPA. The bias is reduced considerably, for example, from +95% to +8% in case of SSMIS-F17 as well as the RMSE. The level of improvement is consistent with the correlation measures. Moreover, the percent bias indicates that PMW precipitation estimates using the IMERG algorithm slightly underestimate the precipitation for all PMW sensors except SSMIS-F18 and conical average.

Maps of correlation and RMSE are shown in Figure 7. They are computed for each 0.25° grid box over the study period to understand the spatial distribution of agreement. Figure 7a shows maps for TMPA-RT and IMERG (MW and IR merged products). The IMERG product exhibits better agreement with the reference across the West Coast, central, and northeast regions. The correlation coefficient is higher for TMPA-RT for the South and East Coast, which are regions mainly impacted by hurricanes and tropical storms. Consistently, the RMSE is significantly reduced for IMERG over the central United States. For IR-only precipitation estimates (Figure 7b), IMERG exhibits significant and noticeable improvement in correlation and RMSE. The central region, South, and East Coast are marked by moderate correlation coefficient and lower RMSE.

Based on Tian et al. (2009), the total error is decomposed into three bias components: estimation error (hit bias), miss-rain bias, and false-rain bias. Figure 8 presents the magnitude of the error components from (a)

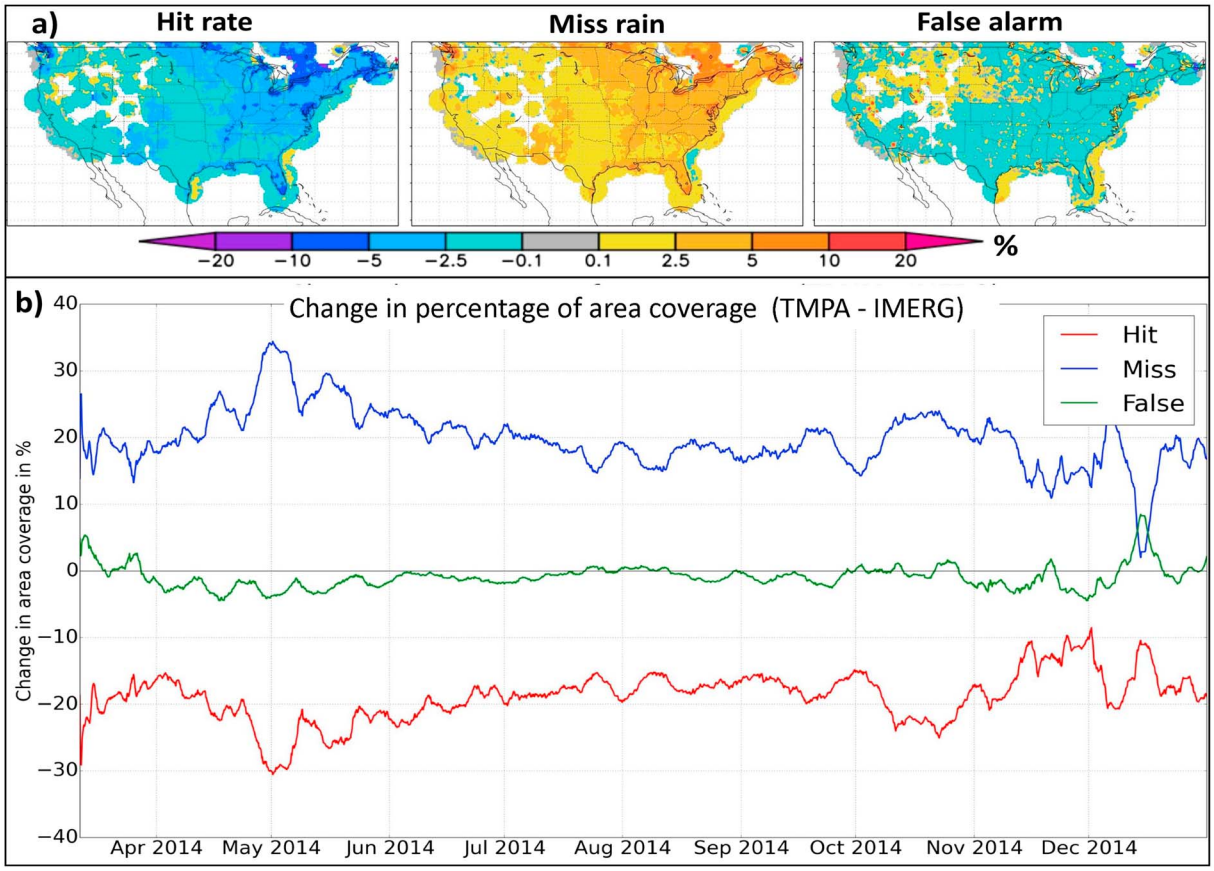

Figure 9. (a) Percentage of improvements related to the occurrence hit rate, miss-rain, and false alarm (by subtracting Integrated Multi-Satellite Retrievals for Global Precipitation Measurement (IMERG) from Tropical Rainfall Measurement Mission-based Multi-satellite Precipitation Analysis real-time product (TMPA-RT)): percentage of occurrence of the three categorical measures during the study period (2014). (b) Change in percentage area coverage of hit, miss, and false alarm between TMPA-RT and IMERG as a function of time.

PMW and (b) IR sensors as identified in TMPA-RT and IMERG. The magnitude of miss-rain bias observed during the entire period in TMPA-RT is considerably mitigated with the IMERG algorithm (Figure 8a). Miss-rain bias is possibly due to short-lived precipitation events missed because of the infrequent revisit of the low Earth orbit satellites on which PMW sensors fly or because of an IR detection issue (stemming from calibration by PMW sensors with deficient detection). Therefore, the implementation of the CMORPH-KF and PERSIANN-CCS schemes in IMERG contributes significantly to improving the miss-rain bias by respectively increasing the contribution of PMW and improving the IR retrieval. PERSIANN-CCS may bring a substantial improvement in the detection of rain with functional structures related to the patch-based approach. As further illustrated in Figure 8b, in regions of IR-based TMPA precipitation estimates both the miss-rain and false-rain biases are substantially reduced in IMERG. As discussed before, this is attributed to use of both morphing and PERSIANN-CCS.

Finally, the level of improvement is also measured as a function of the difference of occurrence and area coverage of the hit rate, miss, and false alarm between the two algorithms. First, the percentage of occurrence of these categorical measures is computed for both algorithms. The difference of occurrence is then calculated by subtracting the percentage of IMERG from its TMPA-RT counterpart. Accordingly, a negative percentage change in hit rate means that IMERG has better hit (detection) capability than TMPA-RT. Figure 9a presents the difference in percentage of frequency of occurrence of hit, miss, and false rain between TMPA-RT and IMERG algorithms. The frequency of miss-rain is lower for the IMERG product, the hit rate is higher, and the false alarm is slightly higher than TMPA-RT in most of the CONUS (Figure 9a). This shows that IMERG demonstrates better performance in reducing the miss-rain rate and increasing the hit rate, in agreement with Figure 8. In case of hit rate and miss-rain, IMERG shows outstanding performance compared to TMPA-RT in

the North and Northeast. This is related to the improved capability of IMERG to remotely sense and estimate both liquid rain and falling snow using the improved GPROF algorithm.

In Figure 9b and similar to the frequency of occurrence hit, miss, and false alarm, the IMERG product shows smaller area coverage for the miss-rain compared to TMPA-RT, larger area of the hit/rain detection, and fairly similar area coverage with the TMPA-RT in case of the false alarm (Figure 9b). In general, the IMERG algorithm demonstrates significant functional improvement for precipitation estimation, particularly with reducing the miss-rain bias related to PMW and IR sensors and largely in decreasing the false-rain bias in the TMPA IR precipitation retrieval. Better understanding about the accuracy, performance, and level of improvement of the IMERG product can be achieved through detailed and comprehensive analysis of the product without altering both the spatial and temporal resolutions. Future work is in progress to produce a ground reference at the native resolution of IMERG product (half-hourly, 0.1° × 0.1°).

4. Conclusion

This study investigates the shift in accuracy in satellite precipitation estimates from the TRMM to the GPM era and demonstrates the advances in the new generation of multisatellite precipitation products. It presents the level of improvement achieved in IMERG multisatellite precipitation product in comparison to its predecessor, TMPA-RT, and at the same spatial and temporal scales. We use the TMPA-RT sensor source identifier as a baseline for the comparison. The MRMS precipitation estimate is utilized as reference data to evaluate both products. The degree of improvement is evaluated by computing the statistical measures for pixel and aggregated precipitation estimates, decomposing the error components and quantifying magnitude of reduction, and investigating the change in frequency of occurrence and area coverage of the three error components. The result of the study can be summarized as follows:

1. The Version 7 TMPA-RT overestimates IR precipitation significantly against MRMS, which is mainly the result of false precipitation and hit bias. The overestimation due to false-rain bias is mitigated in the Version 03 IMERG Late Run product. The algorithm markedly improves the IR precipitation retrieval mainly due to the implementation of CMORPH-KF and PERSIANN-CCS. The GPROF PMW retrieval used in IMERG reduces the miss-rain bias observed in TMPA-RT.
2. In addition to the error magnitude, the occurrence of miss-rain is substantially reduced and the hit rate is improved in IMERG product with respect to both its frequency and area coverage. Related to false precipitation, IMERG does not show significant change from TMPA-RT in terms of frequency of occurrence and area coverage but demonstrates extensive improvement with respect to the magnitude of false-rain bias.

It is noteworthy that the prelaunch version of IMERG shows better performances than the TMPA algorithm which has been matured over the TRMM era. This can be achieved only by a more accurate merging of the multisatellite precipitation products in IMERG relative to TMPA. It is important to recognize that these conclusions are based on a relatively short period of data (1 year) and tested only over the CONUS, indicating that further study using a larger data set at global scale is necessary. Consideration of other factors such as geophysical features, different weather, and climate is essential. More importantly, the impact of the uncertainty induced during spatial and temporal aggregation of IMERG precipitation estimates is not entirely clear. Further study at the native IMERG spatial and temporal scales, using a longer data set, will overcome these limitations.

Appendix A: Performance Measures

Let us assume that S_r is the precipitation estimate by the satellite, R_r the reference (ground truth) precipitation, TB the total bias, HB the hit bias, MB the missed-rain bias, FB the false-rain bias, TH the threshold value, and n the number of sample size. For practical purposes TH can be considered between 0 and 1 mm/d of precipitation (Tian et al., 2009)

$$\mathrm{TB} = S_r - R_r$$

$$\text{If } S_r > \mathrm{TH} \text{ and } R_r > \mathrm{TH}, \text{then } \mathrm{HB} = S_r - R_r \tag{A1}$$

$$\text{If } S_r <= \mathrm{TH} \text{ and } R_r > \mathrm{TH}, \text{then } \mathrm{MB} = S_r - R_r = -R_r \tag{A2}$$

$$\text{If } S_r > \mathrm{TH} \text{ and } R_r <= \mathrm{TH}, \text{then } \mathrm{FB} = S_r - R_r = S_r \tag{A3}$$

Therefore, to evaluate the error, it is important to develop event mask for the respective error components as shown below.

Condition	Error component	Event mask		
		H	M	F
$S_r > \text{TH}$ and $R_r > \text{TH}$	Hit	1	0	0
$S_r <= \text{TH}$ and $R_r > \text{TH}$	Miss	0	1	0
$S_r > \text{TH}$ and $R_r <= \text{TH}$	False	0	0	1
$S_r <= \text{TH}$ and $R_r <= \text{TH}$	No error	0	0	0

If the event masks are denoted as R_h, R_m, and R_f for hit, miss-rain, and false-rain components, respectively, then we can demonstrate that the sum of error components is equal to the total bias.

$$\begin{aligned}\text{HB} + \text{MB} + \text{FB} &= (S_r - R_r)\times R_h + (-R_r)\times R_m + (S_r)\times R_f \\ &= S_r\times R_h - R_r\times R_h - R_r\times R_m + S_r\times R_f \\ &= S_r(R_h + R_f) - R_r(R_h + R_f).\end{aligned}$$

From the event mask matrix above $R_h + R_f = R_h + R_f = 1$ for all conditions except $S_r <= \text{TH}$ and $R_r <= \text{TH}$ ("no error" condition). Thus,

$$\text{HB} + \text{MB} + \text{FB} = S_r\times 1 - R_r\times 1 = S_r - R_r = \text{TB} \tag{A4}$$

Covariance, cov

$$\text{cov}(S_r, R_r) = \sum_{i=1}^{n} \frac{\left(S_r^i - \overline{S}_r\right)\left(R_r^i - \overline{R}_r\right)}{n} \tag{A5}$$

Correlation coefficient, r

$$r(S_r, R_r) = \frac{\text{cov}(S_r - R_r)}{\sigma_S \sigma_R} \tag{A6}$$

root mean square error, RMSE

$$\text{RMSE} = \sqrt{\frac{\sum_{i=1}^{n}\left(S_r^i - R_r^i\right)^2}{n}} \tag{A7}$$

Nash-Sutcliffe model efficiency coefficient, E

$$E = 1 - \frac{\sum_{i=1}^{n}\left(S_r^i - R_r^i\right)^2}{\sum_{i=1}^{n}\left(R_r^i - \overline{R}_r\right)^2} \tag{A8}$$

index of agreement, d

$$d = 1 - \frac{\sum_{i=1}^{n}\left(S_r^i - R_r^i\right)^2}{\sum_{i=1}^{n}\left(\left|S_r^i - \overline{R}_r\right| + \left|R_r^i - \overline{R}_r\right|\right)^2} \tag{A9}$$

Acknowledgments

A. G. and P. E. K. acknowledge support from the National Aeronautics and Space Administration Precipitation Science Program under solicitation NNX16AE39G and from the GPM mission Ground Validation program award NNX16AL23G. W. A. P. acknowledges support from the GPM Mission (Project Scientist, Gail S.-Jackson and GV Systems Manager, Mathew Schwaller) and also Precipitation Measurement Mission (PMM) Science Team funding provided by Ramesh Kakar. We are very much indebted to the team responsible for the MRMS products who provided the data for this study. MRMS data are available at http://mrms.ncep.noaa.gov/data/ and https://wallops-prf.gsfc.nasa.gov/NMQ/index.html. The IMERG and TMPA data were provided by the NASA/Goddard Space Flight Center's PMM and Precipitation Processing System (PPS) teams, which develop and compute IMERG and TMPA as a contribution to GPM and TRMM, respectively, and are archived at the NASA GES DISC (https://pmm.nasa.gov/data-access/downloads/gpm). IMERG and TRMM data can be downloaded from http://pmm.nasa.gov/data-access.

References

Chen, S., Zhang, J., Mullens, E., Hong, Y., Behrangi, A., Tian, Y., … Zhang, X. (2015). Mapping the precipitation type distribution over the CONUS using NOAA/NSSL National Multi-Sensor Mosaic QPE. *IEEE Transactions on Geoscience and Remote Sensing*, *53*(8), 4434–4443. https://doi.org/10.1109/TGRS.2015.2399015

Curtis, S., Crawford, T. W., & Lecce, S. A. (2007). A comparison of TRMM to other basin-scale estimates of rainfall during the 1999 Hurricane Floyd flood. *Natural Hazards*, *43*(2), 187–198. https://doi.org/10.1007/s11069-006-9093-y

Dinku, T., Ceccato, P., Grover-kopec, E., Lemma, M., Connor, S. J., & Ropelewski, C. F. (2007). Validation of satellite rainfall products over East Africa's complex topography. *International Journal of Remote Sensing*, *28*(7), 1503–1526. https://doi.org/10.1080/01431160600954688

Dinku, T., Chidzambwa, S., Ceccato, P., Connor, S. J., & Ropelewski, C. F. (2008). Validation of high-resolution satellite rainfall products over complex terrain in Africa. *International Journal of Remote Sensing*, *29*(14), 4097–4110. https://doi.org/10.1080/01431160701772526

Ebert, E. E., Janowiak, J. E., & Kidd, C. (2007). Comparison of near-real-time precipitation estimates from satellite observations and numerical models. *Bulletin of the American Meteorological Society*, *88*(1), 47–64. https://doi.org/10.1175/BAMS-88-1-47

Gebregiorgis, A. S., & Hossain, F. (2014). Estimation of satellite precipitation error variance using readily available geophysical features. *IEEE Transation Geoscience and Remote Sensing*, *52*, 288–304. https://doi.org/10.1109/TGRS.2013.2238636

Gebregiorgis, A., Kirstetter, P. E., Hong, Y., Carr, N., Gourley, J. J., & Zheng, Y. (2017). Understanding multi-sensor satellite precipitation error structure in level-3 TRMM products. *Journal of Hydrometeorology*, *18*, 285–306. https://doi.org/10.1175/JHM-D-15-0207.1

Gottschalck, J., Meng, J., Rodell, M., & Houser, P. (2005). Analysis of multiple precipitation products and preliminary assessment of their impact on global land data assimilation system land surface states. *Journal of Hydrometeorology*, *6*(5), 573–598. https://doi.org/10.1175/JHM437.1

Hong, K. L. H., Sorooshian, S., & Gao, X. (2004). Precipitation estimation from remotely sensed imagery using an artificial neural network cloud classification system. *Journal of Applied Meteorology*, *43*(12), 1834–1853. https://doi.org/10.1175/JAM2173.1

Hong, Y., Adler, R. F., Hossain, F., Curtis, S., & Huffman, G. J. (2007). A first approach to global runoff simulation using satellite rainfall estimation. *Water Resources Research*, *43*, W08502. https://doi.org/10.1029/2006WR005739

Huffman, G. J., & Bolvin, D. T. (2015). TRMM and other data precipitation data set documentation, mesoscale atmospheric processes laboratory, *NASA Global Change Master Directory Doc.*, 44 pp. http://pmm.nasa.gov/sites/default/files/document_files/3B42_3B43_doc_V7.pdf.

Huffman, G. J., Bolvin, D. T., Nelkin, E. J., Wolff, D. B., Adler, R. F., Gu, G., … Stocker, E. F. (2007). The TRMM Multisatellite Precipitation Analysis (TMPA): Quasi-global, multiyear, combined-sensor precipitation estimates at fine scales. *Journal of Hydrometeorology*, *8*(1), 38–55. https://doi.org/10.1175/JHM560.1

Huffman, G. J., Adler, R. F., Bolvin, D. T., & Nelkin, E. J. (2010). The TRMM Multi-Satellite Precipitation Analysis (TMPA). In M. Gebremichael, & F. Hossain (Eds.), *Satellite rainfall applications for surface hydrology*, (pp. 3–22). New York: Springer. https://doi.org/10.1007/978-90-481-2915-7_1

Huffman, G. J., Bolvin, D. T., Braithwaite, D., Hsu, K., Joyce, R., & Xie, P. (2014). GPM Integrated Multi-Satellite Retrievals for GPM (IMERG) Algorithm Theoretical Basis Document (ATBD) version 4.4. PPS, NASA/GSFC, 30 pp. http://pmm.nasa.gov/sites/default/files/document_files/IMERG_ATBD_V4.4.pdf

Huffman, G. J., Bolvin, D. T., & Nelkin, E. J. (2015). Integrated Multi-Satellite Retrievals for GPM (IMERG) technical documentation. *NASA/GSFC Code*, *612*, 47. http://pmm.nasa.gov/sites/default/files/document_files/IMERG_doc.pdf

Joyce, R. J., & Xie, P. (2011). Kalman filter based CMORPH. *Journal of Hydrometeorology*, *12*, 1547–1563. https://doi.org/10.1175/JHM-D-11-022.1

Kirstetter, P. E., Hong, Y., Gourley, J. J., Chen, S., Flamig, Z., Zhang, J., … Amitai, E. (2012). Toward a framework for systematic error modeling of spaceborne precipitation radar with NOAA/NSSL ground radar-based national mosaic QPE. *Journal of Hydrometeorology*, *13*(4), 1285–1300. https://doi.org/10.1175/JHM-D-11-0139.1

Kirstetter, P. E., Hong, Y., Gourley, J. J., Cao, Q., Schwaller, M., & Petersen, W. (2014). A research framework to bridge from the Global Precipitation Measurement mission core satellite to the constellation sensors using ground radar-based National Mosaic QPE. In L. Venkataraman et al. (Eds.), *Remote sensing of the terrestrial water cycle, AGU Geophysical Monograph Series*. Hoboken, NJ: John Wiley. https://doi.org/10.1002/9781118872086.ch4

Kirstetter, P., Hong, Y., Gourley, J. J., Schwaller, M., Petersen, W., & Cao, Q. (2015). Impact of sub-pixel rainfall variability on spaceborne precipitation estimation: Evaluating the TRMM 2A25 product. *Quarterly Journal of the Royal Meteorological Society*, *141*(688), 953–966. https://doi.org/10.1002/qj.2416

Kirstetter, P. E., Karbalaee, N., Hsu, K., & Hong, Y. (2017). Probabilistic precipitation rate estimates with space-based infrared sensors. *Quarterly Journal of the Royal Meteorological Society*. https://doi.org/10.1002/qj.3243, in press.

Kummerow, C. D., Barnes, W., Kozu, T., Shiue, J., & Simpson, J. (1998). The Tropical Rainfall Measuring Mission (TRMM) sensor package. *Journal of Atmospheric and Oceanic Technology*, *15*(3), 809–817. https://doi.org/10.1175/1520-0426(1998)015%3C0809:TTRMMT%3E2.0.CO;2

Kummerow, C. D., Randel, D. L., Kulie, M., Wang, N. Y., Ferraro, R., Munchak, S. J., & Petkovic, V. (2015). The evolution of the Goddard profiling algorithm to a fully parametric scheme. *Journal of Atmospheric and Oceanic Technology*, *32*(12), 2265–2280. https://doi.org/10.1175/JTECH-D-15-0039.1

Levizzani, V., Amorati, R., & Meneguzzo, F. (2002). A review of satellite-based rainfall estimation methods, European Commission Project MUSIC Rep. EVK1-CT-2000-00058, 66 pp.

Passive Microwave Algorithm Team Facility, PMATF (2014), Global Precipitation Measurement (GPM) mission—Algorithm theoretical basis document (available at http://rain.atmos.colostate.edu/ATBD/ATBD_GPM_Aug1_2014.pdf)

Ruane, A. C., & Roads, J. O. (2007). The diurnal cycle of water and energy over the Continental United States from three reanalyses. *Journal of the Meteorological Society of Japan*, *85A*, 117–143. https://doi.org/10.2151/jmsj.85A.117

Sapiano, M. R. P., & Arkin, P. A. (2008). An inter-comparison and validation of high resolution satellite precipitation estimates with three-hourly gauge data. *Journal of Hydrometeorology*, *10*, 149–166.

Tang, L., Tian, Y., & Lin, X. (2014). Validation of precipitation retrievals over land from satellite-based passive microwave sensors. *Journal of Geophysical Research-Atmospheres*, *119*, 4546–4567. https://doi.org/10.1002/%202013JD020933

Tian, Y., Peters-Lidard, C. D., Choudhury, B. J., & Garcia, M. (2007). Multitemporal analysis of TRMM-based satellite precipitation products for land data assimilation applications. *Journal of Hydrometeorology*, *8*(6), 1165–1183. https://doi.org/10.1175/2007JHM859.1

Tian, Y., Peters-Lidard, C. D., Eylander, J. B., Joyce, R. J., Huffman, G. J., Adler, R. F., … Zeng, J. (2009). Component analysis of errors in satellite-based precipitation estimates. *Journal of Geophysical Research*, *114*(D24), D24101. https://doi.org/10.1029/2009JD011949

Turk, J. T., Mostovoy, G. V., & Anantharaj, V. (2010). The TRMM Multi-satellite Precipitation Analysis (TMPA). In F. Hossain, & M. Gebremichael (Eds.), *Satellite rainfall applications for surface hydrology*, (pp. 3–ss). Springer Verlag.

Willmott, C. J. (1981). On the validation of models. *Physical Geography*, *2*, 184–194.

Wolff, D. B., Marks, D. A., Amitai, E., Silberstein, D. S., Fisher, B. L., Tokay, A., … Pippitt, J. L. (2005). Ground validation for the Tropical Rainfall Measuring Mission (TRMM). *Journal of Atmospheric and Oceanic Technology*, *22*(4), 365–380. https://doi.org/10.1175/JTECH1700.1

Zhang, J., Qi, Y., Langston, C., & Kaney, B. (2011). Radar quality index (RQI) – A combined measure of beam blockage and VPR effects in a national network. *Proceedings of International Symposium on Weather Radar and Hydrology, Exeter, UK, Apr 2011* (Vol. 351, pp. 388–393). Wallingford, UK: IAHS Press.

Zhang, J., Howard, K., Langston, C., Kaney, B., Qi, Y., Tang, L., … Kitzmiller, D. (2015). Multi-Radar Multi-Sensor (MRMS) quantitative precipitation estimation: Initial operating capabilities. *Bulletin of the American Meteorological Society*, *97*(4), 621–637. https://doi.org/10.1175/BAMS-D-14-00174.1